Food Hydrocolloids 163 (2025) 111119

Contents lists available at ScienceDirect

Food Hydrocolloids

journal homepage: www.elsevier.com/locate/foodhyd

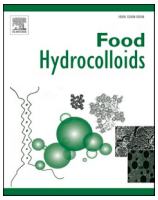

Physicochemical and functional properties of plant proteins before and after extrusion texturization

Ruoshi Xiao, Jenna Flory, Sajid Alavi, Yonghui Li *

Department of Grain Science and Industry, Kansas State University, Manhattan, KS, 66506, USA

ARTICLE INFO

Keywords:
Plant-based proteins
Extrusion process
Texturized proteins
Protein-protein interactions

ABSTRACT

Rapid expansion of animal meat production raises environmental, welfare, biodiversity, and health concerns. Plant-based meat alternatives offer promise in mitigating these issues. Texturized vegetable proteins are key substitutes created through extrusion processing. Our study utilized a pilot-scale twin-screw extruder to texturize raw materials with varying proportions of cold-swelling proteins and heat-swelling proteins. Characterization revealed significant physicochemical and functional changes after extrusion texturization. Results indicated a decrease in α-helix structure accompanied by an increase in β-sheet content after extrusion, suggesting significant conformational changes in protein structures. Solubility tests conducted with different extracting buffers highlighted disulfide bonds as the primary force maintaining fibrous structure integrity. Extrusion resulted in decreased concentration of free amino and sulfhydryl groups, reduced surface hydrophobicity, fluctuating digestibility, water and oil holding capacities, diminished emulsifying and foaming properties, and increased least gelation concentration. Overall, extrusion induced diverse changes in properties, enhancing the suitability of fibrous structures as meat alternatives.

1. Introduction

Animal-based proteins are favored in the food markets due to their desirable taste, complete amino acid composition, and good functionalities for high-quality food production (Ozturk & Hamaker, 2023). However, meat products have significant impact on the anthropogenic environment. Their production processes require substantial water and land resources and contribute to elevated greenhouse gas emissions. Ethical concerns regarding the slaughter of animals have also prompted many consumers to opt for non-animal protein sources (McClements & Grossmann, 2021). Additionally, the transportation of meat products presents challenges due to their perishable nature, necessitating cold environments. During this supply chain, they are susceptible to being disrupted or affected by diseases like swine flu and avian flu (Ozturk & Hamaker, 2023). Besides, some studies have shown that several human diseases such as obesity, type 2 diabetes, cardiovascular disease, stroke, and colorectal cancer have a relationship with the red meat diet (Willett et al., 2019) and the high fat content of meat is also associated with a high-risk factor for human health (Zhang, Zhao, et al., 2022). Animal-based proteins also exhibit lower production efficiency compared to alternative protein sources. As a result, consumer preferences are increasingly shifting toward protein sources that are more environmentally sustainable, economically viable, ethically acceptable, and healthy. Meat alternatives, including plant-based, cell-based (cultured meat), fermentation-based (mycoprotein) (Souza Filho et al., 2019), algae-based, and insect-based sources, have emerged as viable options.

Animal proteins possess a unique muscle structure that is absent in plant-based proteins, making it challenging to achieve a comparable mouthfeel, texture, and sensory characteristics. Various special processing techniques, such as extrusion, shear-structuring (shear cell), 3D printing, electrospinning, and freeze-structuring, can be employed to create fibrous anisotropic structures (Ozturk & Hamaker, 2023). Shear cell technology is a relatively new method but with relatively lower processing capacity compared to other methods (Ozturk & Hamaker, 2023). 3D printing involves layering a paste-like mixture of protein powder, water, and additives to form a structure. However, it is limited to thermoplastic formulations with fewer ingredients and is more suitable for liquid-like materials because it lacks the shear force to handle solid-like materials (McClements & Grossmann, 2022). Electrospinning uses electricity to create micro- and nano-scale fibers, but faces challenges with plant proteins, which often have a globular structure that

* Corresponding author.
E-mail addresses: rosexiao@ksu.edu (R. Xiao), jflory09@ksu.edu (J. Flory), alavi@ksu.edu (S. Alavi), yonghui@ksu.edu (Y. Li).

https://doi.org/10.1016/j.foodhyd.2025.111119
Received 30 September 2024; Received in revised form 16 January 2025; Accepted 20 January 2025
Available online 21 January 2025

resists spinning (Nieuwland et al., 2014). Freeze structuring mimics the texture of meat by freezing a protein emulsion and removing ice crystals to form a porous fibrous structure. However, this technology requires additional steps, such as freeze drying or cross-linking, to stabilize the structure (Ozturk & Hamaker, 2023). Among these, extrusion technology is the most mature and extensively studied method for producing meat analogues, with research dating back to the late 1980s and early 1990s. It offers several advantages, including low processing costs, continuous production, efficient energy utilization, and high output (Zhang et al., 2023). Additionally, this technique is compatible with a wide range of protein materials, and the resulting products typically require minimal additional processing.

According to the differences in moisture content, the extrusion method can be divided into two types: low-moisture extrusion and high-moisture extrusion. Low-moisture extrusion, conducted at moisture levels of 30–40%, produces texturized vegetable proteins (TVP), which require rehydration or further processing before use, but have a longer shelf life). High-moisture extrusion, performed at moisture levels of about 60–65%, yields high moisture meat analogues (HMMA) with a meat-like texture that can be used without further hydration needs but have a shorter shelf-life due to their high moisture content (Akdogan, 1999; Webb et al., 2023a, 2023b). Zhang and Ryu (2023) compared pea protein isolate extruded under high (HMMA) and low (TVP) moisture conditions. HMMA showed superior physical and textural properties, including integrity and texture profiles, with significant differences in disulfide bond content between the extrudates.

Moreover, significant differences in the physicochemical and functional properties of protein samples are evident when comparing their states before and after the extrusion process. Gao et al. (2023) investigated wheat germ protein as a raw material and observed that extrusion led to a reduction in free sulfhydryl groups and surface hydrophobicity of the proteins. Conversely, protein solubility, emulsification capacity, and digestibility improved. Similarly, Zhang et al. (2022) studied the combined extrusion of soybean protein and wheat gluten under high-moisture conditions. Their findings indicated an increase in β-sheet structure and enhanced rehydration properties of the extrudates. Consistent with these results, Meng et al. (2022) reported a decrease in surface hydrophobicity and an increase in β-sheet content in proteins subjected to extrusion.

In addition to processing techniques, the selection of appropriate raw materials is crucial for extrusion. Soybean proteins have long been favored due to their balanced amino acid composition and widespread consumer acceptance (Sui et al., 2021). Pea proteins are gaining attention for their cost-effectiveness, lack of allergens, non-genetically modified nature, and cholesterol-free properties (Liu et al., 2020; McCarthy et al., 2016). Wheat gluten, a coproduct of wheat starch isolation, offers favorable viscoelastic and thermal coagulation characteristics (Zhang, Zhao, et al., 2022). The advantages of several other protein sources are summarized in Table 1. These proteins possess unique functionalities and can be categorized into cold-swelling proteins (CS) and heat-swelling proteins (HS) based on their different water absorption capacity, viscosity peak time, and least gelation concentration (LGC). Specifically, proteins exhibiting a high WAI (>4.0 g/g), rapid viscosity peak formation (<4 min), and less LGC were classified as CS, while those demonstrating different characteristics were referred to as HS (Flory et al., 2023).

Table 1
Different protein sources and their advantages.

Protein sources	Advantages	References
Soybean protein	Contains all amino acids essential to human nutrition, with less saturated fat and no cholesterol	Xiao (2008)
Pea protein	Contains high levels of lysine, a good source of bioactive peptides, low allergenicity	Shanthakumar et al. (2022)
Wheat gluten	High content of Gln and hydroxyl amino acids (ca 10%), good viscoelastic property	Zhang, Zhao, et al. (2022)
Rice protein	High lysine content of glutelin, hypoallergenic, higher nutrition quality	Amagliani et al. (2017)
Mung bean protein	High essential amino acid content (such as leucine, lysine and phenylalanine/tyrosine), high protein digestibility	Zhu et al. (2018)
Lupin protein	Contains a significant content of lysine and other essential amino acids, bioactive peptides	Lemus-Conejo et al. (2023)

In our previous study, we utilized samples with varying CS ratio to determine which formulation would result in improved texture and enhance the quality and sensory attributes of plant-based meat. We observed that after the low-moisture extrusion process, samples with higher CS ratios exhibited a greater tendency for crosslinking, leading to a porous internal structure with reduced layering. Conversely, samples with lower CS ratios resulted in a denser, more stratified extrudate structure (Flory et al., 2023). However, the exact reasons behind this phenomenon remain unclear. To investigate the underlying mechanism, we conducted further experiments focused on protein property analysis.

Therefore, in this study, analyses of both raw materials and resulting extruded products were performed to elucidate the underlying mechanisms involved in extrusion texturization. The analyses included assessments of protein secondary structure, solubility, free amino content, free sulfhydryl content, surface hydrophobicity, *in vitro* protein digestibility (IVPD), water holding capacity (WHC), oil holding capacity (OHC), emulsifying activity index (EAI), emulsifying stability index (ESI), foaming capacity (FC), and LGC. Our objective is to comprehend changes in physicochemical properties and functionalities of the plant proteins during extrusion and provide fundamental insights into the effects of CS/HS ratio and extrusion processes on protein structures.

2. Materials and methods

2.1. Materials

The samples used in this study remained the same as those detailed in the research conducted by Flory et al. (2023), comprising six treatments with varying cold-swelling protein ratios: 0% CS, 30% CS, 40% CS, 50% CS, 60% CS, and 90% CS. These samples consisted of blends of soybean protein isolate (SPI), two variants of soybean protein concentrate (Arcon F and Arcon S SPC), soybean flour, pea protein isolate (PPI), and wheat gluten (Gluten). Based on the report from Flory et al. (2023), the SPI, SPC Arcon S type, and PPI could be identified as CS proteins, while SPC Arcon F type and Gluten were classified as HS proteins. Although samples with varying cold swelling ratios utilized different protein ingredients, the overall protein content across all samples remained relatively consistent (around 71.48%). Both individual ingredients and the resulting raw-material blends, as well as the texturized proteins from the treatments, were utilized in the subsequent experiments. The protein samples mentioned were all ground into fine powder using a coffee grinder and subsequently stored in a refrigerator at 4 °C for later use. Trypsin from porcine pancreas (13,000–20,000 BAEE units/mg protein), α-chymotrypsin from bovine pancreas (≥40 units/mg protein), and protease from *Streptomyces griseus* (≥3.5 units/mg protein) were purchased from Sigma-Aldrich (St. Louis, MO, USA). Urea, dithiothreitol (DTT), sodium dodecyl sulfate (SDS), thiourea, 3-[(3-cholamidopropyl) dimethylammonio]-1-propanesulfonate (CHAPS), sodium phosphate dibasic, sodium dihydrogen phosphate anhydrous, bovine serum albumin (BSA), sodium dioxide (NaOH), hydrochloric acid (HCl), Coomassie Brilliant blue G 250, methylene blue, tris(hydroxymethyl)aminomethane (Tris), glycine, ethylenediaminetetraacetic acid (EDTA), 5, 5′-dithiobis(2-nitrobenzoic acid), β-mercaptoethanol, trichloroacetic acid (TCA), and leucine were also purchased from Sigma-Aldrich. Phosphoric acid, chloroform, and 2,4,6-trintrobenzenesulfonic acid were purchased from Fisher Scientific (Waltham, MA, USA).

2.2. FTIR spectroscopy

FTIR spectroscopy, a method for analyzing the secondary structure of proteins, was conducted using a PerkinElmer Spectrum 400 FT-IR/FTNIR Spectrometer (PerkinElmer, Inc., Waltham, MA, USA) equipped with an attenuated total reflectance cell (ATR) accessory. The samples were kept on diamond crystal and were secured tightly with a clamp for the analysis. Each sample underwent 64 scans within the range of 400–4000 cm^{-1}, with a 4 cm^{-1} interval. The relative areas of the amide I region (1600–1700 cm^{-1}) were determined using OriginPro 2016 software (OriginLab, Inc., Northampton, MA, USA) (Gao et al., 2023). The determination of α-helix, β-sheet, β-turn, and random coil structures in the protein secondary structure with the distribution ratio were quantified using the method described by Kong and Yu (2007).

2.3. Solubility

The protein solubility was determined using different extracting buffers to indirectly analyze the protein-protein interactions, following the method from Liu and Hsieh (2008) with modifications. 200 mg sample was mixed with 10 mL of each extractant and shaken for 2 h (300 rpm) at room temperature. The supernatant was obtained by centrifugation at 8000*g* for 15 min. The protein content in the supernatant was quantified using the Bradford assay (Kielkopf et al., 2020). The extractants include: (1) **Isoelectric focus buffer (IEF)**: 8M urea and 50 mM dithiothreitol (DTT) and 2% (w/v) sodium dodecyl sulfate (SDS) + 2M thiourea +2% (w/v) 3-[(3-Cholamidopropyl) dimethylammonio]-1-propanesulfonate (CHAPS) in phosphate buffer (U + D + S + T + C + P); (2) **IEF w/o Urea**: 50 mM DTT and 2% (w/v) SDS + 2M thiourea +2% (w/v) CHAPS in phosphate buffer (D + S + T + C + P); (3) **IEF w/o DTT**: 8M urea and 2% (w/v) SDS + 2M thiourea +2% (w/v) CHAPS in phosphate buffer (U + S + T + C + P); (4) **IEF w/o Urea and DTT**: 2% (w/v) SDS + 2M thiourea +2% (w/v) CHAPS in phosphate buffer (S + T + C + P); (5) **IEF w/o Thiourea, SDS, and CHAPS**: 8M urea and 50 mM DTT in phosphate buffer (U + D + P); (6) **PB**:100 mM phosphate buffer, pH 7.5 (P). Protein solubility was assessed by comparing the protein content in the supernatant to that of the samples, presenting it as a ratio.

2.4. Determination of free amino groups

The amount of free amino groups indicates the degree of hydrolysis in samples and helps identify the formation of covalent bonds during the extrusion process. The method outlined by Groβmann et al. (2021) was used to determine free amino content with some modifications. 0.5 mL of a sample solution, with a concentration of 4 mg/mL and dissolved in a 1% (w/v) SDS solution, was combined with 4 mL of 0.2125 M phosphate buffer (pH 8.2, the mixture of 4.5 mL 0.2125 M NaH_2PO_4 and 100 mL 0.2125 M Na_2HPO_4) and 4 mL of 0.1% (v/v) 2,4,6-trinitrobenzene sulfonic acid (TNBS). This suspension was then incubated in a 50 °C water bath at 200 rpm for 1 h in darkness. Following the hour-long reaction, 8 mL of 0.1 N HCl was introduced to the solution, which was then stored at room temperature for 30 min. The resulting supernatant was obtained by centrifugation at 8000*g* for 10 min, and its absorbance was measured using a double beam spectrometer (VWR UV-6300PC, Radnor, PA, USA) at 340 nm. Additionally, L-leucine solutions were prepared following the same procedure, but with varying concentrations (ranging from 0 to 2.4 mM), to establish a standard curve.

2.5. Determination of free sulfhydryl groups and surface hydrophobicity

The study of inter- and intramolecular sulfhydryl groups change is important for identifying the structural changes caused by extrusion process. The determination of free sulfhydryl content followed the method described by Hao et al. (2022). A 75 mg sample was dispersed in 10 mL of Tris-Gly-urea buffer (containing 0.086 mol/L Tris, 0.09 mol/L glycine, 0.004 mol/L EDTA, and 8 mol/L urea) and shaken overnight. For free sulfhydryl content determination, 1 mL sample was mixed with 4 mL Tris-Gly buffer and 0.05 mL Ellman's reagent (4 mg/mL), shaken for 15 min in the dark, centrifuged (8000×*g*, 8 min), and absorbance measured at 412 nm. Blanks were used for correction. For total sulfhydryl content determination, 1 mL sample was mixed with 4 mL Tris-Gly buffer and 0.05 mL β-mercaptoethanol, shaken for 1 h, and precipitated with 10 mL 12% TCA. The precipitate was washed, resuspended in 10 mL Tris-Gly buffer, and reacted with 0.04 mL Ellman's reagent for 15 min. After centrifugation, absorbance at 412 nm was measured. The equation used for calculating was as follows:

$$\text{SH content } (\mu\text{M SH / g}) = \frac{73.53 \times A_{412} \times \text{D}}{C} \quad (1)$$

$$\textit{Disulfide bonds content } (\mu M / g) = (\textit{Total SH content} - \textit{Free SH content}) / 2 \quad (2)$$

Where A_{412} was the final absorbance at 412 nm; D was the dilution factor (5 was used in free sulfhydryl content determination and 10 was used in total sulfhydryl content determination); C was the sample concentration (mg/mL); 73.53 was derived from $10^6/(1.36 \times 10^4)$ where 1.36×10^4 was the molar absorptivity of Ellman' reagent and 10^6 was for conversions from the molar basis to the μM/mL basis and from mg sample to g sample.

The determination of surface hydrophobicity (H_0) provides insight into the hydrophobic interactions within samples, which play an important role in the formation and stabilization of protein structures. In this study, H_0 was measured using SDS binding method, in accordance with the approach detailed by Tang et al. (2021). Protein sample (10 mg) was mixed with 40 mL of 0.1 mmol/L SDS buffer for 1 h, then dialyzed in distilled water for 48 h using SnakeSkin™ tubing (MW cut-off: 3.5 kDa). The dialyzed solution volume was recorded, and 10 mL was mixed with 25 mL of chloroform and 5 mL of methylene blue (24 mg/L). After shaking for 5 min, the mixture was centrifuged at 2500×*g* for 15 min. The absorbance of the lower layer was measured at 655 nm using a UV–Vis spectrometer. SDS concentration was quantified using a standard curve to estimate surface hydrophobicity based on SDS binding.

2.6. In vitro protein digestibility

Protein digestibility, used to assess potential bioavailability and protein quality, was determined according to the method from Martínez-Velasco et al. (2018) with some modifications. A 30 mL sample solution containing 6.25 mg of protein per milliliter was prepared, followed by adjustment of the pH to 8.00 (±0.02) using 1 M HCl and/or NaOH. Simultaneously, a multienzyme solution was prepared consisting of 1.6 mg trypsin, 3.1 mg α-chymotrypsin, and 1.3 mg protease per milliliter of distilled water. The pH of the enzyme solution was similarly adjusted and maintained at 8.00 (±0.02). After mixing 3 mL of the enzyme solution with the sample at 37 °C for 10 min, the pH drop was recorded using a pH meter. The equation was based on the literature of Tinus et al. (2012):

$$\textit{Protein digestibility}\% = 65.66 + 18.10 \times \Delta pH_{10\ min} \quad (3)$$

where ΔpH_{10min} was the change of pH in 10 min from the initial pH 8.0.

2.7. Functional properties

The water and oil holding capacity were quantified following the approach detailed by Espinosa-Ramírez and Serna-Saldívar (2016) with modifications. For water holding capacity determination, 0.25 g of the sample (W_0) was combined with 7.5 mL of distilled water in a 15 mL centrifuge tube (W_2) and shaken for 30 min at 300 rpm. After centrifugation at 4500*g* for 15 min, the tube was inverted for 5 min to drain

water residues, and the final weight was recorded (W_1). Water holding capacity was calculated using the formula:

$$WHC\ (g\ water\ /\ g\ protein) = \frac{W_1 - W_2 - W_0}{W_0} \quad (4)$$

Similarly, for oil holding capacity determination, a 0.25 g sample (O_0) was mixed with 7.5 mL of soybean oil in a 15 mL centrifuge tube (O_2). After shaking, centrifugation, and inversion to drain the oil, the final precipitate weight was recorded (O_1). The oil holding capacity was calculated as same:

$$OHC\ (g\ oil\ /\ g\ protein) = \frac{O_1 - O_2 - O_0}{O_0} \quad (5)$$

The determination of both emulsifying capacity was conducted in accordance with a turbidimetric method detailed by Espinosa-Ramírez and Serna-Saldívar (2016) with some modifications. The procedure involved adding 0.25 g of samples to 25 mL of 100 mM phosphate buffer (pH = 7) and stirring until a uniform solution was achieved. Next, 25% (v/v) soybean oil was dispersed into the solution, followed by homogenization using homogenizer (Polytron PT 2500 E, Kinematica AG, Switzerland) at 14,000 rpm for 1 min at room temperature. After homogenization, 50 μL of the solution was mixed with 2.95 mL of 0.1% (w/v) SDS buffer and vortexed. The absorbance of the diluted emulsion was then measured at 500 nm (A_0) and again after 10 min (A_{10}). The Emulsification Activity Index (EAI) and Emulsion Stability Index (ESI) were subsequently calculated using the following formulas:

$$T = 2.303 \times \frac{A_0}{L} \times D \quad (6)$$

$$EAI\ (m^2\ /\ g) = \frac{2 \times T}{\varphi \times C \times 1000} \quad (7)$$

$$ESI\ (min) = \frac{A_0}{A_0 - A_{10}} \times t \quad (8)$$

where T is the turbidity of emulsion, A is the absorbance at 500 nm, D is dilution factor, L is the path length of light (m), φ is the oil volume fraction, C is the protein concentration in the dispersion (mg/mL), t is 10 min.

Proteins serve as stabilizers at gas-liquid interfaces, forming foams that are crucial for the texture and appearance of various products. The foaming capacity (FC), which is the main parameter measured in this experiment, is commonly expressed as the ratio of the foam volume to the original protein suspension volume (%). FC is typically related to the solubility of protein in water. Foaming stability (FS) refers to the retention of FC over time, with stability measured as the FC values at different time points. The FC and FS of samples were assessed using the protocol described by Shen et al. (2021). Gelation occurs when proteins denature, unfold, and aggregate to form a three-dimensional network that traps water and other components, which is also important for food applications. The least gelation concentration (LGC) is the minimum protein concentration (%) required to form a stable gel. The LGC of the samples was determined using the method described by Shen and Li (2021).

2.8. Statistical analysis

The experiments were performed in at least duplicate, and the results were presented as mean values ± standard deviations (SD). Statistical analysis was carried out using IBM SPSS Statistics software (version 27.0.1., Armonk, NY, USA). One-way analysis of variance (ANOVA) was conducted, followed by Tukey's test for multiple comparisons to compare means. Statistical significance was determined at $P < 0.05$. Principal Component Analysis (PCA) was conducted using OriginPro 2016 software (OriginLab, Inc., Northampton, MA, USA) to analyze the relationships among different properties and samples (raw ingredients, raw material blends, and TVPs).

3. Results and discussion

3.1. Protein secondary structure

Protein secondary structure was determined using Fourier Transform Infrared (FTIR). In FTIR spectroscopy, various functional groups present within analyzed samples exhibit unique absorption patterns at distinct wavelengths, resulting in characteristic peaks in the spectrum. The amide I band, spanning from 1600 to 1700 cm^{-1}, is particularly informative as it reflects the structural arrangement of protein components, primarily associated with the C=O stretch vibration, and is highly sensitive to changes in secondary structure (Gao et al., 2023). Hence, our study focused solely on analyzing this specific band. Quantification of changes in secondary structure was performed by assessing the peak areas of each fitted sub-peak within the amide I band. Table 1 presents the distribution of α-helix, β-sheet, β-turn, and random coil structures in the protein secondary structure. The distribution ratio was quantified using the method described by Kong and Yu (2007). Distinct absorption peak wavelengths are associated with each of these structural elements: α-helix (1654-1658 cm^{-1}, 1660-1666 cm^{-1}), β-sheet (1623-1629 cm^{-1}, 1631-1643 cm^{-1}, 1689-1698 cm^{-1}), β-turn (1666-1668 cm^{-1}, 1674-1687 cm^{-1}), and random coil structure (1646-1650 cm^{-1}). These specific wavelengths facilitate the identification and quantification of different protein secondary structures, providing valuable insights into structural alterations induced by sample formulation and extrusion texturization.

In Table 2, a varied trend in α-helix content was observed with increasing CS levels in raw-material blends. Samples with 0% CS (R) and 40% CS (R) exhibited notably higher α-helix content (33.20% and 39.86%, respectively), surpassing other raw samples significantly ($P < 0.05$). This phenomenon can be attributed to the higher proportion of wheat gluten present in these two samples compared to others. By combining the findings from Table S1 in the supplementary material, it becomes apparent that wheat gluten displayed the highest α-helix content among the proteins (46.82%). The α-helix structure, owing to its

Table 2
Protein secondary structures from FTIR.

Samples	Protein secondary structure ratio %			
	α-Helix	β-Sheet	β-Turn	Random coil
0% CS(R)	33.20 ± 3.09^{b}	60.67 ± 3.32^{cd}	6.13 ± 0.23^{bcd}	0.00 ± 0.00^{e}
30% CS (R)	27.65 ± 0.00^{cd}	57.51 ± 0.00^{de}	3.24 ± 0.00^{d}	11.60 ± 0.00^{d}
40% CS (R)	39.86 ± 2.56^{a}	57.13 ± 1.38^{de}	3.01 ± 1.19^{d}	0.00 ± 0.00^{e}
50% CS (R)	22.45 ± 0.49^{de}	63.58 ± 0.50^{bc}	3.26 ± 0.23^{d}	10.72 ± 0.21^{d}
60% CS (R)	23.05 ± 0.92^{de}	51.23 ± 0.05^{f}	6.79 ± 0.31^{bc}	18.93 ± 1.18^{b}
90% CS (R)	25.98 ± 4.82^{cde}	57.74 ± 0.90^{de}	5.86 ± 3.72^{bcd}	10.42 ± 0.20^{d}
0% CS(T)	22.95 ± 1.03^{de}	71.84 ± 0.11^{a}	5.21 ± 0.91^{bcd}	0.00 ± 0.00^{e}
30% CS(T)	20.52 ± 1.27^{e}	71.86 ± 1.15^{a}	7.62 ± 0.11^{b}	0.00 ± 0.00^{e}
40% CS(T)	11.40 ± 0.20^{f}	57.91 ± 0.90^{de}	5.43 ± 0.24^{bcd}	25.26 ± 0.94^{a}
50% CS(T)	25.81 ± 3.20^{cde}	55.18 ± 0.39^{e}	3.64 ± 0.09^{d}	15.37 ± 2.90^{c}
60% CS(T)	23.87 ± 1.72^{de}	62.14 ± 3.06^{bc}	13.98 ± 1.33^{a}	0.00 ± 0.00^{e}
90% CS(T)	30.26 ± 3.34^{bc}	65.56 ± 2.21^{b}	4.19 ± 1.12^{cd}	0.00 ± 0.00^{e}

Note: Results are expressed as mean ± SD (n = 2). Different letters indicate significant differences in the same column ($P < 0.05$). CS means cold-swelling protein, (R) means the raw-material blends, and (T) means the texturized proteins or extrudates.

extensive hydrogen-bonding network, offers an advantage in non-polar solvents, which correlates with the low solubility of wheat gluten in most research (Gao et al., 2023). Furthermore, the predominant protein secondary structure in the raw material blends was the β-sheet structure. Analysis from Table S1 revealed that, apart from wheat gluten, nearly all raw ingredients exhibited a substantial proportion of β-sheet structure. In the research conducted by Zhang, Zhao, et al. (2022), native PPI demonstrated a high content of β-sheet structure at 48.33%. Similarly, Li et al. (2023) illustrated that various types of SPI predominantly possessed a β-sheet structure (ranging from 37.80% to 42.56%). This finding was also corroborated by Meng et al. (2022). Additionally, the content of β-sheet and β-turn structures remained relatively stable across different levels of CS. Notably, 60% CS (R) sample exhibited a significant increase ($P < 0.05$) in random coil content compared to other CS levels, possibly due to its variation in ingredient composition.

After extrusion texturization, there was an increase in the content of β-sheet and β-turn structures in samples compared to the raw material blends, while the content of α-helix and random coil structures fluctuated. Initially, α-helix content decreased in samples with 0%–40% CS (T), but then exhibited a non-significant increase in samples with 50%–90% CS (T). The most significant reduction was observed in 40% CS (T) (decreased by 28.46%, $P < 0.05$). This decline could be attributed to the intense shear and thermal stresses experienced during extrusion, leading to protein unfolding and reorientation. However, the increase in α-helix content in samples containing higher levels of cold-swelling proteins suggests that there may be less alteration in protein structure after extrusion texturization. This observation is consistent with most previous studies, where the α-helix structure either decreased or did not undergo significant changes after extrusion, even when samples were composed of different protein sources (Gao et al., 2023; Li et al., 2023; Meng et al., 2022; Zhang, Zhao, et al., 2022).

The majority of protein secondary structure in the texturized protein samples were also comprised β-sheet structures, accounting for around 55.18%–71.86%. This prevalence of β-sheet structures may be attributed to their stability in aggregates (Zhang, Zhao, et al., 2022). After the extrusion process, there was a significant increase in β-sheet content, although some samples exhibited slight decreases (e.g., 50% CS (T)) or remained relatively stable (e.g., 40% CS (T)). Under the extreme conditions of extrusion texturization, irreversible protein denaturation occurred, leading to the transition from α-helix to β-sheet structure (Gao et al., 2023). Zhang, Zhao, et al. (2022) demonstrated that the α-helix structure decreased while the β-sheet structure underwent a significant increase after extrusion, suggesting the stretching of polypeptide chains to promote the formation of an ordered fibrous structure. However, the relationship between the content of α-helix or β-sheet structure and the quality of fibrous end products remains unclear. Notably, the 60% CS (T) displayed a significant increase in β-turn content after extrusion (7.19%), indicating the formation of more flexible protein structures. Additionally, the 40% CS (T) exhibited a significant increase in random coil structures post-extrusion, suggesting a transformation from ordered to disordered structures induced by the extrusion process.

The changes in protein secondary structures during the extrusion process can provide valuable insights into changes in protein functionalities. For instance, Othmeni et al. (2024) investigated the relationship between protein secondary structure and foaming properties of pea protein. Their findings showed that α-helix structure might negatively affect the foaming expansion while the increase of β-sheet and random coil structures might improve the foaming stability. Similarly, Bai et al. (2016) revealed the relationship between protein secondary structure, solubility, and digestibility. They found a positive relationship between α-helix and random coil with protein solubility and digestibility but a negative relationship between β-sheet and these properties. However, the solubility, protein digestibility, and foaming properties observed in our extruded samples were not fully consistent with the results above, which may be due to the difference in protein source and processing conditions.

3.2. Solubility

An important physicochemical property that influences many other functions of proteins is their solubility. Protein solubility plays a critical role during food production, storage, and consumption (Grossmann & McClements, 2023). However, most texturized samples often exhibit extremely low solubility in water, necessitating an investigation into the bonds or interactions that predominantly influence solubility. To address this, we employed multiple solvents containing various functional reagents to disrupt non-covalent or covalent bonds and enhance the solubility of the samples. This approach allowed us to identify the bonds formed during the extrusion texturization process that contribute most to the observed low solubility. Several solvents were utilized to dissolve the six texturized samples: phosphate buffer to extract proteins in their native state, can possibly disrupt the electrostatic interaction, urea to disrupt hydrogen bonding, and SDS, CHAPS, and thiourea for breaking down hydrophobic interactions (Liu & Hsieh, 2008) (Table 3). Additionally, DTT was employed to cleave disulfide bonds. The solubility results of the extrudates with increasing CS ratio are shown in Fig. 1.

According to Flory et al. (2023), the protein solubility of the raw material blends with different CS ratios ranged from 20.04% to 46.20% in water. But after extrusion texturization, the solubility of the texturized proteins in phosphate buffer (native state) notably decreased, with values ranging only from 0.64% to 1.74%. However, upon the addition of various chemical buffers, their solubility dramatically increased, changing from average 1.05% (in PB) to 80.93% (in IEF buffer). This phenomenon indicates that many chemical bonds or interactions were formed in proteins during extrusion texturization, resulting in aggregate formation. The IEF buffer, containing all the reactive agents, achieved the highest solubility for these samples, ranging from 70.72% to 88.95%. Remarkably, the 0% CS (T) exhibited the highest solubility (88.95%), which gradually decreased with increasing CS ratios. This trend suggests that higher cold swelling ratios may contribute to reduced solubility, possibly due to differences in protein structure alterations during extrusion.

When urea was excluded from the solvent, solubility decreased across all CS levels compared to the solubility of samples in IEF buffer. This decline underscores the importance of hydrogen bonding in maintaining protein aggregates. With the increase of CS ratios, reductions fluctuated, with the extrudates with 0% CS and 40% CS presenting relatively lower reductions (13.96% and 12.22%) compared to other extrudates. However, the extrudate with 50% CS experienced the highest decrease (31.92%). These differences were not only caused by the extrusion process but also by the variation in formulations of samples with different cold swelling ratios.

Excluding DTT, the reducing agent, from the solvent, resulted in a more significant decrease on solubility ($P < 0.05$). On average, solubility decreased by approximately 60.08%, indicating a strong response to

Table 3
Effect of extracting solutions on protein interactions.

Extracting solution	The specific interactions that are disrupted by reagents		
	Disulfide bonding	Hydrogen bonding	Hydrophobic interaction
Isoelectric focus buffer (IEF)	✓	✓	✓
IEF w/o urea	✓		✓
IEF w/o DTT		✓	✓
IEF w/o urea and DTT			✓
IEF w/o thiourea, SDS, and CHAPS	✓	✓	
PB			

Note: IEF buffer: isoelectric focus buffer, contains all the reagents including urea, DTT, SDS, thiourea, CHAPS, and phosphate buffer; DTT: dithiothreitol; SDS: sodium dodecyl sulfate; CHAPS: 3-[(3-cholamidopropyl) dimethylammonio]-1-propanesulfonate; PB: phosphate buffer.

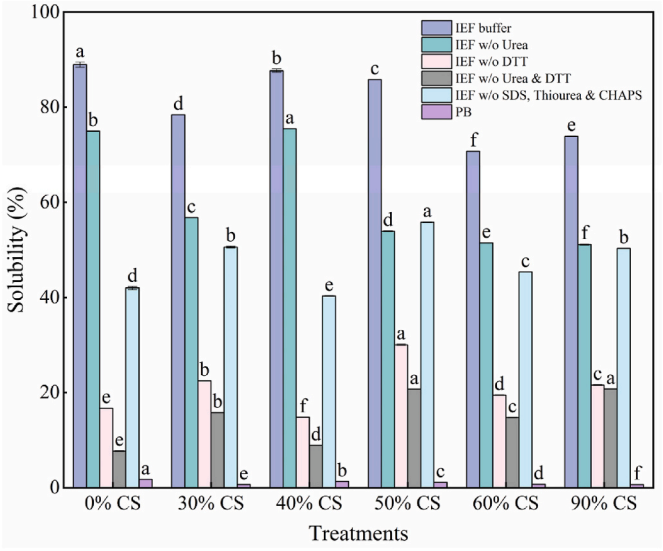

Fig. 1. Protein solubility in different tailored buffers. Note: Different letters indicate significant differences in solubility from the same buffer ($P < 0.05$). CS means cold-swelling protein and (T) means the texturized proteins or extrudates. IEF buffer: isoelectric focus buffer, contains all the reagents including urea, DTT, SDS, thiourea, CHAPS, and phosphate buffer; DTT: dithiothreitol; SDS: sodium dodecyl sulfate; CHAPS: 3-[(3-cholamidopropyl) dimethylammonio]-1-propanesulfonate; PB: phosphate buffer.

disulfide bond disruption. Notably, the solubility of the texturized samples with 0% and 40% CS experienced drops of 72.24% and 72.88%, respectively, while the decrease in other samples was around 50%. This phenomenon may also be attributed to differences in their formulation, as only these two samples contained wheat gluten, which is rich in disulfide bonds (Table S3), as confirmed by the test of free -SH group determination (Table 2). Conversely, PPI and SPI (or SPC) may have more non-covalent bond sites and a greater tendency to form hydrogen bonding.

The combination of excluding both urea and DTT (IEF w/o Urea & DTT) further reduced solubility across all CS levels, suggesting synergistic effects of disrupting both hydrogen and disulfide bonds. The extrudate with 0% CS experienced the most decrease, with an 81.29% reduction, followed by the extrudate with 40% CS experienced 72.88% reduction. This phenomenon confirms the reason explained above.

Excluding SDS, thiourea, and CHAPS (IEF w/o SDS, thiourea & CHAPS) led to a moderate reduction in solubility across CS levels, decreasing by 33.52% compared to the solubility in IEF buffer alone, indicating the role of hydrophobic interactions in protein solubility. Interestingly, the reduction in solubility observed in IEF w/o SDS, thiourea & CHAPS buffer was higher than that in IEF w/o Urea buffer, suggesting that hydrophobic interactions may contribute more to protein aggregation during extrusion texturization compared to hydrogen bonding. But both hydrophobic interactions and hydrogen bonding have the function to remain constant during extrusion (Liu & Hsieh, 2008). From the results above, we can infer a sequence of driving forces for different covalent or non-covalent bonds during extrusion texturization: disulfide bond > hydrophobic interaction > hydrogen bonding. The most important chemical bond which may maintain the integrity and fibrous of the extrudates was disulfide bond, affecting solubility the most. However, other studies employing similar methods with slight modifications to determine the solubility of extrudates have reported different findings. Zhang and Ryu (2023) found out that the most critical force driving aggregation in texturized PPI samples was hydrophobic interactions, followed by disulfide bonds. Zhang, Zhao, et al. (2022), investigating a soybean protein and wheat gluten blend under high-moisture extrusion, and Osen et al. (2015), studying PPI under high-moisture extrusion, identified hydrogen bonding as the dominant interaction during the extrusion process, with disulfide bonding playing a secondary role. The differences in these studied may be attributed to the sample composition or the conditions of extrusion processing, such as temperature and moisture levels.

3.3. Determination of free amino groups

The free amino content of samples serves as a crucial indicator of their nutritional value and functionality in food products, offering insight into the Maillard reaction initiation and peptide bonds formation, and other chemical linkages formation involving -NH_2 during extrusion. The results of the amount of free amino groups in samples are presented in Table 4.

Within raw material blends, there was a clear increasing trend in free amino content with increased CS ratios, ranging from 3.47 to 6.90 mmol/g protein. This trend suggests that cold swelling proteins facilitate the exposure of free amino groups from protein matrices, possibly due to their more native stage and higher initial free amino content in the original ingredients (Table S2). Specifically, the free amino groups in the 50% CS (R) and 90% CS (R) samples were significantly ($P < 0.05$) higher than in other samples. This difference may be attributed to variations in sample formulation, notably, these two samples were the only ones that included PPI in their formulations, which had the highest free amino content among all the raw ingredients.

After extrusion texturization, there was a significant decrease in free amino content compared to raw material blends ($P < 0.05$). This reduction could be attributed to thermal degradation, Maillard reactions (which occur between amino groups and reducing sugars), or other processing-induced transformations leading to the loss of free amino groups and their conversion into other compounds. During extrusion processing, concomitant processes such as protein denaturation, starch dextrinization, lipid oxidation, cellulose degradation, the Maillard

Table 4
Protein free amino content, free sulfhydryl content, surface hydrophobicity, and *in vitro* protein digestibility (IVPD).

Samples	Free amino content (mmol/g protein)	Free sulfhydryl content (μmol/g protein)	Surface hydrophobicity (μg SDS/mg protein)	IVPD (%)
0% CS (R)	3.47 ± 0.05^{g}	2.21 ± 0.10^{de}	59.73 ± 1.96^{c}	85.21 ± 0.26^{g}
30% CS (R)	4.68 ± 0.02^{e}	2.66 ± 0.12^{bcd}	64.14 ± 1.20^{b}	87.38 ± 0.26^{e}
40% CS (R)	4.88 ± 0.02^{d}	2.61 ± 0.02^{cd}	64.28 ± 0.35^{b}	87.47 ± 0.13^{e}
50% CS (R)	5.53 ± 0.03^{b}	3.12 ± 0.24^{ab}	54.83 ± 0.97^{d}	89.37 ± 0.26^{c}
60% CS (R)	5.29 ± 0.05^{c}	2.83 ± 0.03^{abc}	69.05 ± 1.67^{a}	88.83 ± 0.26^{d}
90% CS (R)	6.90 ± 0.05^{a}	3.24 ± 0.04^{a}	57.27 ± 0.55^{cd}	91.18 ± 0.51^{a}
0% CS (T)	1.75 ± 0.02^{i}	2.03 ± 0.02^{e}	35.80 ± 1.72^{g}	86.11 ± 0.00^{f}
30% CS (T)	3.11 ± 0.05^{h}	1.99 ± 0.03^{e}	38.41 ± 1.35^{g}	89.64 ± 0.13^{c}
40% CS (T)	1.67 ± 0.03^{i}	2.06 ± 0.06^{e}	37.14 ± 1.44^{g}	86.20 ± 0.13^{f}
50% CS (T)	3.90 ± 0.05^{f}	2.03 ± 0.14^{e}	42.22 ± 0.83^{f}	90.37 ± 0.13^{b}
60% CS (T)	3.19 ± 0.03^{h}	1.96 ± 0.03^{e}	42.00 ± 0.14^{f}	89.46 ± 0.13^{c}
90% CS (T)	3.85 ± 0.06^{f}	1.32 ± 0.04^{f}	49.10 ± 1.29^{e}	89.82 ± 0.13^{c}

Note: Results are expressed as mean ± SD (n = 2). Different letters indicate significant differences in the same column ($P < 0.05$). CS means cold-swelling protein, (R) means the raw-material blends, and (T) means the texturized proteins or extrudates.

reaction, and water redistribution collectively influence the final product's attributes, encompassing its color, flavor (Zhang et al., 2019).

Notably, the extrudates with 0% CS and 40% CS exhibited the lowest free amino content compared to other texturized samples. This difference may also be attributed to the distinct formulation of these two samples, as they were the only ones with the addition of wheat gluten, which contained the lowest free amino content (3.07 mmol/g protein) among the ingredients. Conversely, the free amino content showed no significant difference between native PPI and extrudates in the study conducted by Osen et al. (2015), suggesting that the reactions involving free amino group was not evident.

In the study of Ding et al. (2019), they used transglutaminase to form isopeptide bonds within protein structure to increase the cross-linking and significantly decrease the amount of free amino groups in proteins. They observed that with increasing transglutaminase concentration, which decreased free amino group concentration, both emulsifying and foaming capacity were improved obviously, but a careful balance of cross-linking formation was required to obtain good emulsion and foam stability. However, in our study, the decrease of free amino groups did not lead to better emulsifying or foaming properties, which may be because multiple factors interact in complex ways to affect protein functionality.

3.4. Determination of free sulfhydryl groups

The free sulfhydryl content of proteins is a vital parameter that reflects the extent of disulfide bond formation and protein structural changes, which can imply the denaturation degree of protein structure. In this study, the free sulfhydryl content of samples was examined and presented in Table 4. The free sulfhydryl content exhibited a moderate increase trend with varying CS levels in raw material blends, indicating increased accessibility of sulfhydryl groups when samples contained a larger proportion of cold-swelling proteins. As shown in Table S3, the cold-swelling proteins (SPI, SPC (Arcon S), and PPI) had a higher free sulfhydryl content, which also corroborates the results above. Notably, 90% CS (R) exhibited the highest free sulfhydryl content (3.24 μmol/g protein) followed by 50% CS (R) (3.12 μmol/g protein), which may result from the high SPI content in these two samples.

After extrusion, the values of the sulfhydryl content were all decreased significantly from the average 2.78 μmol/g protein to 1.90 μmol/g protein ($P < 0.05$). Particularly, the extrudate with 90% cold swelling ratio experienced the most significant decrease, dropping to 1.32 μmol/g protein after extrusion. The mechanical shear forces during extrusion can cause physical disruption to proteins, exposing sulfhydryl groups. Subsequently, the high temperatures involved in extrusion can lead to the oxidation of sulfhydryl groups, resulting in their conversion to disulfide bonds, which aligns with the inference drawn from the solubility test (Mosibo et al., 2022). This oxidative process can decrease the concentration of free sulfhydryl groups in the sample. Comparative results can also be observed in previous studies that used wheat gluten or a combination of PPI, SPI, gluten, and corn starch as raw ingredients (Gao et al., 2023; Zhang & Ryu, 2023). Conversely, samples comprised of SPI, PPI, or even oat protein concentrate only, after the extrusion process, showed an increase in free sulfhydryl content (Li et al., 2023; Pöri et al., 2022; Zhang, Zhao, et al., 2022). These differences may be attributed to the variation in raw materials and different extrusion conditions. Since under certain conditions, the extrusion process can break down disulfide bonds and unfold the protein structure in the samples. In addition, extrudates with the increasing CS levels demonstrated a decrease in free sulfhydryl content, indicating that different cold swelling ratios in samples can be affected differently by the thermal process.

Changes in the amount of disulfide bonds and free sulfhydryl groups will also affect the protein functionalities. Yang et al. (2023) demonstrated the ultrasound coupled with weak alkali treatment effectively cleaved disulfide bonds, releasing more free sulfhydryl groups in protein samples, which enhanced their emulsifying properties. However, Othmeni et al. (2024) reported that the increase in disulfide bond content improved the foaming properties of protein samples. These findings highlight that specific structural modifications of proteins need to be targeted to their future application.

3.5. Surface hydrophobicity

Surface hydrophobicity is a key parameter that reflects changes in protein conformation and structure. It also significantly influences the interfacial behavior of proteins, including emulsifying and foaming properties. The surface hydrophobicity results are exhibited in Table 4. The surface hydrophobicity of raw material blends exhibited a mixed pattern with varying CS levels with an average of 61.55 μg SDS/mg protein. Notably, 60% CS (R) demonstrated the highest surface hydrophobicity of 69.05 μg SDS/mg protein, indicating its higher exposure of hydrophobic regions on the protein surface. The ingredients for 60% CS (R) also had a relatively high surface hydrophobicity ranged from 53.28 to 77.65 μg SDS/mg protein, as shown in Table S2. However, the surface hydrophobicity of the samples with 50% and 90% CS only had an average value of 56.05 μg SDS/mg protein. This phenomenon may result from the inclusion of pea protein isolate in their formulation, which had the lowest surface hydrophobicity of 50.69 μg SDS/mg protein among the raw ingredients.

After extrusion texturization, the surface hydrophobicity of samples showed a significant decrease compared to pre-extrusion samples (from 61.55 to 40.78 μg SDS/mg protein, $P < 0.05$). This decrease may be due to the temperature and shearing forces inside the extrusion process that led to the denaturation and aggregation of proteins. As proteins aggregate, the hydrophobic components may become buried deeper within the protein structure driven by hydrophobic interactions, resulting in lower hydrophobicity. Additionally, saccharides can combine with the protein samples after the extrusion process, resulting in an increase in hydrophilic groups, which may also affect the surface hydrophobicity of extrudates (Cheng et al., 2022). These results are consistent with those obtained in the study by Gao et al. (2023), where the surface hydrophobicity of wheat gluten samples all experienced a dramatic decrease after extrusion, even under different extrusion conditions. Similar results were observed in the study by Meng et al. (2022). Additionally, extrudates with higher CS levels demonstrated a slight increase in surface hydrophobicity, ranging from 35.80 to 49.80 μg SDS/mg protein, suggesting that variations in protein formulations may affect protein aggregation or structural rearrangement during extrusion. The 0% CS (T) may experience a more extensive protein modification and aggregation under the extrusion condition.

3.6. In vitro protein digestibility

In vitro protein digestibility (IVPD) is a critical parameter for assessing the nutritional quality and bioavailability of protein-rich foods. In this study, we used three different enzymes to hydrolyze the samples, simulating the digestion process under conditions resembling the intestinal environment. In Table 4, raw material blends with higher cold swelling ratios demonstrated higher IVPD, ranging from 85.21% to 91.18%, indicating enhanced protein digestibility with increasing cold swelling ratio. This trend suggests that the CS proteins have better native structures and higher accessibility of proteolytic enzymes to peptide bonds, thereby promoting protein digestion.

After extrusion texturization, the IVPD of samples showed moderate changes compared to raw material blends. The majority of the samples became more digestible after extrusion process, except for 40% CS (T) and 90% CS (T) samples, which decreased to 86.20% and 89.82%, respectively. In addition, the extrudate with 50% CS exhibited the highest IVPD post-extrusion (90.37%), indicating the potential synergistic effects of sample formulation and extrusion on protein digestibility.

The observed increase in digestibility can be attributed to protein denaturation induced by the extrusion process, which can expose (through unfolding) reactive sites to digestive proteases. Additionally, the moisture and thermal conditions in the extruder may lead to starch gelatinization, allowing the release of proteins from the protein-starch matrix, potentially enhancing protein digestibility. Moreover, extrusion may degrade anti-nutrients that affect protein digestibility, facilitating better enzyme access to substrates (Omosebi et al., 2018). The studies by Gao et al. (2023) and Omosebi et al. (2018), which employed similar methods to determine IVPD in wheat gluten and soybean protein samples before and after extrusion process, support the notion that the extrusion enhances enzyme accessibility by exposing active sites that were previously embedded within the three-dimensional protein structure of the raw materials, thereby increasing the digestibility of the extrudates. However, the extrusion process may also lead to protein aggregation and form a crosslinked protein matrix, inhibiting the enzymatic access to protein structure. In addition, the significant reduction in water solubility of the samples may limit enzyme-protein interactions, potentially decreasing protein digestibility.

3.7. Functional properties

3.7.1. Water and oil holding capacity

The behavior of extruded products in aqueous environments is elucidated by their hydration properties, with the water holding capacity (WHC) being a key factor. The porosity and cell size of samples can be inferred from the value of WHC (Lin et al., 2002). The oil holding capacity (OHC) measures the amount of fat that can be absorbed per gram of protein, showing the affinity of samples for lipid. Both high WHC and high OHC contribute to maintaining the juiciness, tenderness, and mouthfeel of food. However, WHC is more commonly used to evaluate high-moisture foods, whereas high OHC is typically used to assess batters, binders in emulsion-based comminuted meat products, or plant-based alternatives (Day et al., 2022). The results were collected in Table 5.

The WHC of raw materials demonstrated an increasing trend from 1.62 g water/g protein to 4.69 g water/g protein, except for 50% CS (R) containing only 2.32 g water/g protein. This variation may be attributed to the significantly lower WHC of its ingredients like SPC (F) and PPI (Table S4). These WHC results of raw ingredients align with findings from Webb et al.(2023a, 2023b) and indicate that the protein structure or subunits of ingredients can result in different functionalities, thereby affecting WHC values. After extrusion, samples with a cold-swelling protein proportion above 30% showed a decrease in WHC. This suggests that samples with a lower proportion of cold-swelling proteins may experience an increase in air cells and porosity after extrusion. The extrusion process induces the unfolding proteins, leading to the exposure of additional hydrophilic groups, thereby facilitating potential interactions with water molecules (Mosibo et al., 2022). However, samples with higher levels of cold-swelling proteins may not benefit as much from the extrusion process and may even cause the destruction of the sponge-like structure already present in their raw materials. Different protein sources may undergo varied changes in structure when subjected to the extrusion process. Conversely, some samples showed higher WHC compared to raw materials in previous research (Samard and Ryu, 2019). The extrudate with 90% (R) showed the most significant decrease in WHC after extrusion, suggesting a more severe modification. This result aligns with findings by Samard and Ryu (2019) and Zhang and Ryu (2023), indicating that extrudates with higher PPI content may lead to lower WHC values due to a less sponge-like structure after extrusion, hindering water absorption, and the reduction in WHC was found to increase the springiness and chewiness of the samples. Similarly, the findings from Webb et al. (2023b) showed a consistent relationship between WHC values and texture analysis data, demonstrating that the decrease in WHC of samples led to increased hardness and chewiness. This parameter change may result in a firmer and denser texture in the final meat analogues.

All samples exhibited relatively lower oil holding capacity compared to the values of water holding capacity. The OHC of raw material blends showed a slight increasing tendency from 0.82 g oil/g protein to 0.96 g oil/g protein with increasing CS%, except for 50% CS (R) with only 0.59 g oil/g protein. This observation may be attributed to the formulation of this sample, where PPI also had the lowest OHC value, suggesting a reduced presence of non-polar amino acids (Table S4). After extrusion texturization, the OHC values of majority of extrudates significantly increased, while 40% CS (T) and 60% CS (T) showed a slight decrease compared to the raw material blends ($P < 0.05$). These results may arise from the dissociation of proteins, which expose non-polar amino acid side chains to a greater extent, facilitating interactions with oil molecules (Mosibo et al., 2022). In addition, the porous microstructures of extrudates may better trap oil droplets, increasing OHC. The TVP samples with higher WHC are suitable for adding into foods such as soups or gravies, which require high water retention, while those with higher OHC are better used for sausages, salad dressings, or meat extenders (Samard & Ryu, 2019).

3.7.2. Emulsifying properties

Emulsifying properties encompass both the ability to form droplets during homogenization and, once the emulsion is formed, their ability to maintain stability and resist changes over time (Chen et al., 2011). The emulsifying activity index (EAI) and emulsifying stability index (ESI) are crucial parameters that determine the emulsifying properties of proteins, influencing the applicability of samples in various food and industrial applications. In Table 5, the EAI of raw materials had a fluctuating trend ranging from 8.44 m^2/g to 11.41 m^2/g. Notably, the sample with 50% CS had the highest EAI (11.41 m^2/g) followed by the sample with 30% CS (10.82 m^2/g). However, the EAI values decreased after the extrusion process, ranging from 1.59 m^2/g to 6.50 m^2/g,

Table 5
Water holding capacity (WHC), oil holding capacity (OHC), emulsifying properties, and leas gelation concentration (LGC).

Samples	WHC (g water/g material)	OHC (g oil/g material)	EAI (m^2/g)	ESI (min)	LGC (%)
0% CS(R)	1.62 ± 0.01^{i}	0.82 ± 0.00^{f}	8.44 ± 0.13^{d}	15.99 ± 0.43^{g}	18^{d}
30% CS(R)	2.77 ± 0.03^{e}	0.85 ± 0.00^{ef}	10.82 ± 0.26^{b}	19.10 ± 0.94^{f}	20^{b}
40% CS(R)	3.23 ± 0.12^{c}	0.94 ± 0.01^{c}	10.05 ± 0.26^{c}	20.47 ± 0.18^{d}	20^{b}
50% CS(R)	2.32 ± 0.03^{g}	0.59 ± 0.02^{g}	11.41 ± 0.05^{a}	21.77 ± 0.88^{ef}	17^{e}
60% CS(R)	3.65 ± 0.03^{b}	0.96 ± 0.01^{c}	9.72 ± 0.02^{c}	22.84 ± 0.80^{e}	17^{e}
90% CS(R)	4.69 ± 0.02^{a}	0.93 ± 0.05^{cd}	10.01 ± 0.47^{c}	21.34 ± 0.64^{ef}	18^{d}
0% CS(T)	2.55 ± 0.03^{f}	0.89 ± 0.04^{de}	1.59 ± 0.02^{i}	58.81 ± 2.27^{a}	19^{c}
30% CS(T)	3.01 ± 0.01^{d}	1.04 ± 0.00^{b}	6.50 ± 0.10^{e}	14.78 ± 0.58^{g}	20^{b}
40% CS(T)	2.76 ± 0.01^{e}	0.84 ± 0.00^{f}	1.84 ± 0.20^{i}	40.60 ± 0.11^{b}	20^{b}
50% CS(T)	1.98 ± 0.02^{h}	1.03 ± 0.00^{b}	3.73 ± 0.18^{g}	32.92 ± 0.91^{d}	$>20^{a}$
60% CS(T)	2.98 ± 0.02^{d}	0.89 ± 0.00^{d}	4.54 ± 0.45^{f}	21.19 ± 2.00^{ef}	$>20^{a}$
90% CS(T)	2.97 ± 0.02^{d}	1.19 ± 0.00^{a}	2.75 ± 0.10^{h}	36.18 ± 2.07^{c}	19^{c}

Note: Results are expressed as mean ± SD (n = 2). Different letters indicate significant differences in the same column ($P < 0.05$). CS means cold-swelling protein, (R) means the raw-material blends, and (T) means the texturized proteins or extrudates, EAI means emulsifying activity index and ESI means emulsifying stability index.

indicating the poor emulsion ability of extrudates. The sample with 30% CS had the highest EAI among the texturized samples (6.50 m^2/g). The formation of protein aggregates during the extrusion process led to the low solubility of the extrudates, resulting in their poor emulsion ability. The proteins may not dissolve well in water, making it difficult for them to act as effective emulsifiers. This result contrasts with previous studies where some samples exhibited better emulsification ability after extrusion (Gao et al., 2023; Zhang, Zhao, et al., 2022). The differences may stem from variations in sample formulation or different extrusion conditions used.

The ESI of raw materials had a slight increase trend based on the gradient of cold swelling ratio, ranging from 15.99 min to 22.84 min, while the ESI of extrudates exhibited a decreasing trend from 58.81 min to 32.92 min except for 30% CS (T) and 60% CS (T), which had the lowest values of 14.78 min and 21.19 min, respectively. Interestingly, after extrusion, the ESI increased in most samples except for 30% CS (T) and 60% CS (T), which were the only two containing only soybean protein and flour in their formulation. This result aligns with the study by Gao et al. (2023).

3.7.3. Foaming properties

Foam formation can provide a range of unique textures, which are characteristic of many foods, including cakes, bread, ice cream, and confectionery products (Foegeding et al., 2006). The foaming capacity (FC) of both raw materials and extrudates was evaluated to assess their suitability for various food applications. FC was measured at the 0-min mark when the foam was initially made (Fig. 2 and Fig. S1 in the supplementary material). The FC of raw materials ranged from relatively high, ranging from 81.67% to 100.50%, with 40% CS (R) showing the highest FC value. After a 90-min period, only 0% CS (R) and 40% CS (R) experienced the most significant decrease of around 20%, while 50% CS (R) and 90% CS (R) maintained the highest FC at 75%. This result underscores the good foaming capacity of PPI.

After extrusion process, the FC of extrudates dropped dramatically to the average of 10.86%, with 30% CS (T) and 60% CS (T) showing relatively higher values (20.00% and 26.67%, respectively). However, after only a 30 min period, the FC of 30% CS and 60% CS decreased to 0%, while other samples still retained some foam. After another 15 min, only 0% CS (T) and 30% CS (T) had a FC of 1.67%, but by the 60-min mark, all extrudates had lost their foam. Good solubility is a decisive condition for good foaming capacity. The irreversible thermal denaturation of proteins during the extrusion process resulted in a dramatic decrease in sample solubility, leading to the low FC of the extrudates. This finding aligns with the study by Gao et al. (2023), which also observed similar changes in FC after extrusion. Materials with a higher FC are advantageous in certain food production processes. For instance, aerated or foamed products, such as liquids (e.g., beer, sparkling wine, carbonated soft drinks, coffee drinks), semi-solids (e.g., ice cream, whipped cream, aerated desserts), and solids (e.g., bread, cake, breakfast cereals, aerated chocolate bars), are favored in the human diet due to their appealing appearance and distinctive sensory qualities (Amagliani et al., 2021).

3.7.4. Least gelation concentration

Least gelation concentration is one of the most commonly used parameters to measure gelling ability. Proteins with a lower LGC exhibit greater gelling ability. The LGC of raw materials was from 17% to 20%, with 30% CS (R) and 40% CS (R) exhibiting the highest values, indicating their poor ability to form a gel. Samples with a higher proportion of CS proteins demonstrated better gelation ability. Among the raw ingredients, CS proteins also displayed low LGC values (Table S4), consistent with findings from studies by Webb et al. (2023a, 2023b) and Flory et al. (2023). After the extrusion process, the texturized samples either had larger LGC values or maintained similar values compared to the raw materials, ranging from 19% to above 20% (Table 5). This phenomenon may be attributed to the extrusion process leading to the formation of a large proportion of protein aggregates, resulting in folded protein structures. These folded structures were less conducive to absorbing water and trapping it to form a gel-like product. Notably, both 50% CS (T) and 60% CS (T) exhibited the largest LGC values, both exceeding 20%.

3.7.5. Principal component analysis

Principal component analysis was conducted to elucidate the relationships between diverse physicochemical and functional properties and the samples. The analysis revealed that the first (PC1) and second (PC2) principal components collectively explained 55.71% of the total variance in the dataset. In the PCA plot (Fig. 3.), samples forming clusters denote associated characteristics, while those positioned distantly indicate distinct features. Notably, most TVPs and raw material blends were separated primarily along PC1, whereas differentiation based on lower (0%–40% CS) and higher (50%–90% CS) cold-swelling protein ratios occurred along PC2, illustrating sample disparities. 0% CS (R), 30% CS (R), 40% CS (R), PPI, and wheat gluten demonstrated positive associations with foaming capacity, *in vitro* protein digestibility, and β-turn structure. However, wheat gluten exhibited weaker

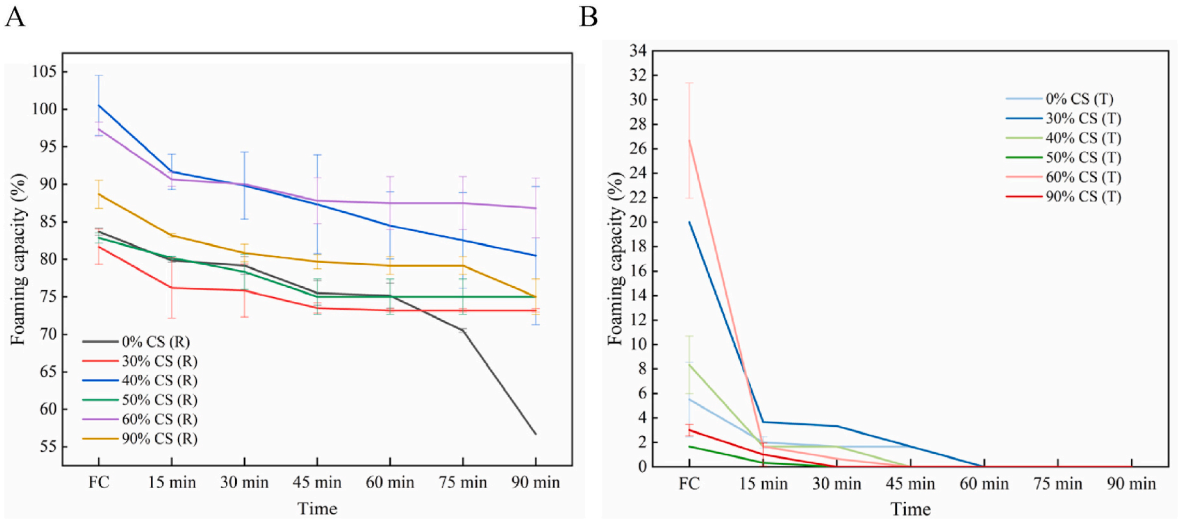

Fig. 2. Foaming properties of raw materials and texturized proteins. Note: A: (R) means the raw-material blends, B: (T) means the texturized proteins or extrudates. CS means cold-swelling protein.

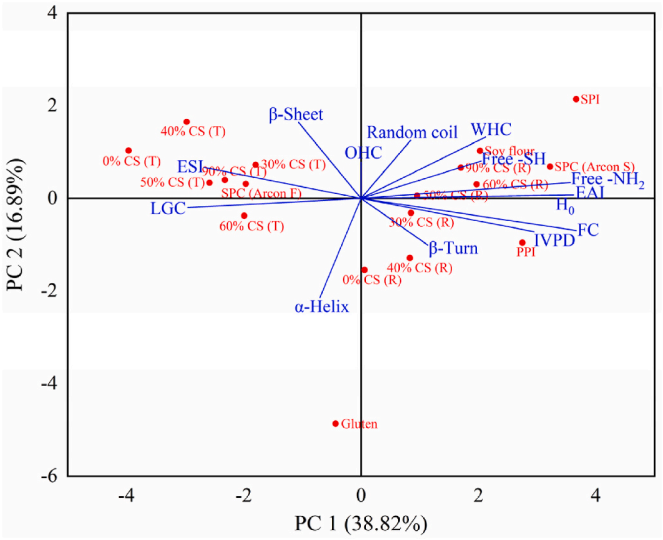

Fig. 3. Principal component analysis (PCA) biplot. Note: This figure describes the relationship among different properties and different samples. SPI means soy protein isolate, SPC (Arcon F or Arcon S) means soy protein concentrate (Arcon F or Arcon S), PPI means pea protein isolate, Gluten means wheat gluten. CS means cold-swelling protein, (R) means the raw-material blends, and (T) means the texturized proteins or extrudates. Protein secondary structures: α-helix, β-sheet, β-turn, random coil. Free -NH_2: free amino content; Free -SH: free sulfhydryl content; H_0: surface hydrophobicity; IVPD: *in vitro* protein digestibility; WHC: water holding capacity; OHC: oil holding capacity; EAI: emulsifying activity index; ESI: emulsifying stability index; FC: foaming capacity; LGC: least gelation concentration.

associations with the analyzed properties compared to other samples. Conversely, raw material blends with higher cold-swelling protein ratios (50%–90%), SPI, SPC (Arcon S), and soy flour had a positive correlation with random coil structure, water holding capacity, free sulfhydryl content, free amino content, emulsifying activity index, and surface hydrophobicity. SPC (Arcon F) and most TVP samples were positively associated with β-sheet structure, emulsifying stability index, and least gelation concentration, whereas weaker connections were observed for 0% CS (T) and 40% CS (T). This phenomenon demonstrates that the extrusion process induced changes in the protein structure of TVP samples, resulting in different properties.

4. Conclusions

In conclusion, this study investigated physicochemical properties of texturized protein samples with different cold swelling ratios before and after extrusion. Higher CS ratios in raw material blends correlated with elevated amino content, sulfhydryl content, digestibility, WHC, and ESI, indicating the higher water affinity of cold-swelling proteins.

Extrusion induced significant structural and functional changes. Protein secondary structures shifted, with α-helix content decreasing and β-sheet content increasing. Solubility decreased largely in the native state, driven by disulfide bond formation, contributing to stable fibrous structures. Reductions in free amino and sulfhydryl contents indicated cross-linking and Maillard reactions, while surface hydrophobicity and digestibility varied with CS ratios. Functional properties such as emulsification and foaming were reduced due to denaturation and aggregation, and the gelation ability of extrudates was limited.

These findings highlight the impact of high-temperature, high-shear extrusion on protein structure and functionality, offering valuable insights into protein-protein interactions and the mechanisms of texturization. While this study focused on functional property changes, further exploration of molecular mechanisms using advanced tools like molecular modeling is recommended. Additionally, varying extrusion parameters such as moisture levels, temperature, and screw speeds could provide a more comprehensive understanding of their effects on protein behavior. These insights are critical for optimizing extrusion processes and developing tailored applications for texturized vegetable proteins in diverse industries.

CRediT authorship contribution statement

Ruoshi Xiao: Writing – review & editing, Writing – original draft, Visualization, Validation, Methodology, Investigation, Formal analysis, Data curation. **Jenna Flory:** Writing – review & editing, Investigation. **Sajid Alavi:** Writing – review & editing, Resources, Methodology, Funding acquisition, Conceptualization. **Yonghui Li:** Writing – review & editing, Supervision, Resources, Project administration, Methodology, Investigation, Funding acquisition, Conceptualization.

Declaration of competing interest

The authors declare that there is no known conflict of interest.

Acknowledgments

This is Contribution No. 24-270-J from the Kansas Agricultural Experimental Station. This work was supported in part by the USDA Pulse Crop Health Initiative project (0439200), USDA National Institute of Food and Agriculture Hatch project (7003330), Kansas Soybean Commission, and a Kansas State University Global Food Systems seed grant.

Appendix A. Supplementary data

Supplementary data to this article can be found online at https://doi.org/10.1016/j.foodhyd.2025.111119.

Data availability

Data will be made available on request.

References

Akdogan, H. (1999). High moisture food extrusion. *International Journal of Food Science and Technology, 34*(3), 195–207. https://doi.org/10.1046/j.1365-2621.1999.00256.x

Amagliani, L., O'Regan, J., Kelly, A. L., & O'Mahony, J. A. (2017). Composition and protein profile analysis of rice protein ingredients. *Journal of Food Composition and Analysis, 59*, 18–26. https://doi.org/10.1016/j.jfca.2016.12.026

Amagliani, L., Silva, J. V. C., Saffon, M., & Dombrowski, J. (2021). On the foaming properties of plant proteins: Current status and future opportunities. *Trends in Food Science & Technology, 118*, 261–272. https://doi.org/10.1016/j.tifs.2021.10.001

Bai, M., Qin, G., Sun, Z., & Long, G. (2016). Relationship between molecular structure characteristics of feed proteins and protein in vitro digestibility and solubility. *Asian-Australasian Journal of Animal Sciences, 29*(8), 1159–1165. https://doi.org/10.5713/ajas.15.0701

Chen, F. L., Wei, Y. M., & Zhang, B. (2011). Chemical cross-linking and molecular aggregation of soybean protein during extrusion cooking at low and high moisture content. *LWT - Food Science and Technology, 44*(4), 957–962. https://doi.org/10.1016/j.lwt.2010.12.008

Cheng, Y.-H., Mu, D.-C., Feng, Y.-Y., Xu, Z., Wen, L., Chen, M.-L., & Ye, J. (2022). Glycosylation of rice protein with dextran via the Maillard reaction in a macromolecular crowding condition to improve solubility. *Journal of Cereal Science, 103*, Article 103374. https://doi.org/10.1016/j.jcs.2021.103374

Day, L., Cakebread, J. A., & Loveday, S. M. (2022). Food proteins from animals and plants: Differences in the nutritional and functional properties. *Trends in Food Science & Technology, 119*, 428–442. https://doi.org/10.1016/j.tifs.2021.12.020

Ding, X., Zeng, N., Zhang, G., Pan, J., Hu, X., & Gong, D. (2019). Influence of transglutaminase-assisted ultrasound treatment on the structure and functional properties of soy protein isolate. *Journal of Food Processing and Preservation, 43*(11), Article e14203. https://doi.org/10.1111/jfpp.14203

Espinosa-Ramírez, J., & Serna-Saldívar, S. O. (2016). Functionality and characterization of kafirin-rich protein extracts from different whole and decorticated sorghum genotypes. *Journal of Cereal Science, 70*, 57–65. https://doi.org/10.1016/j.jcs.2016.05.023

Flory, J., Xiao, R., Li, Y., Dogan, H., Talavera, M. J., & Alavi, S. (2023). Understanding protein functionality and its impact on quality of plant-based meat analogues. *Foods, 12*(17), 3232. https://doi.org/10.3390/foods12173232

Foegeding, E. A., Luck, P. J., & Davis, J. P. (2006). Factors determining the physical properties of protein foams. *Food Hydrocolloids, 20*(2), 284–292. https://doi.org/10.1016/j.foodhyd.2005.03.014

Gao, C., Jia, J., Yang, Y., Ge, S., Song, X., Yu, J., & Wu, Q. (2023). Structural change and functional improvement of wheat germ protein promoted by extrusion. *Food Hydrocolloids, 137*, Article 108389. https://doi.org/10.1016/j.foodhyd.2022.108389

Grossmann, L., & McClements, D. J. (2023). Current insights into protein solubility: A review of its importance for alternative proteins. *Food Hydrocolloids, 137*, Article 108416. https://doi.org/10.1016/j.foodhyd.2022.108416

Großmann, K. K., Merz, M., Appel, D., Thaler, T., & Fischer, L. (2021). Impact of peptidase activities on plant protein hydrolysates regarding bitter and umami taste. *Journal of Agricultural and Food Chemistry, 69*(1), 368–376. https://doi.org/10.1021/acs.jafc.0c05447

Hao, L., Sun, J., Pei, M., Zhang, G., Li, C., Li, C., Ma, X., He, S., & Liu, L. (2022). Impact of non-covalent bound polyphenols on conformational, functional properties and *in vitro* digestibility of pea protein. *Food Chemistry, 383*, Article 132623. https://doi.org/10.1016/j.foodchem.2022.132623

Kielkopf, C. L., Bauer, W., & Urbatsch, I. L. (2020). Bradford assay for determining protein concentration. *Cold Spring Harbour Protocols, 2020*(4), Article 102269. https://doi.org/10.1101/pdb.prot102269

Kong, J., & Yu, S. (2007). Fourier Transform infrared spectroscopic analysis of protein secondary structures. *Acta Biochimica et Biophysica Sinica, 39*(8), 549–559. https://doi.org/10.1111/j.1745-7270.2007.00320.x

Lemus-Conejo, A., Rivero-Pino, F., Montserrat-de la Paz, S., & Millan-Linares, M. C. (2023). Nutritional composition and biological activity of narrow-leafed lupins (*Lupinus angustifolius* L.) hydrolysates and seeds. *Food Chemistry, 420*, Article 136104. https://doi.org/10.1016/j.foodchem.2023.136104

Li, L., Huang, Y., Liu, Y., Xiong, Y., Wang, X., Tong, L., Wang, F., Fan, B., & Bai, X. (2023). Relationship between soybean protein isolate and textural properties of texturized vegetable protein. *Molecules, 28*(22). https://doi.org/10.3390/molecules28227465. Article 22.

Lin, S., Huff, H. E., & Hsieh, F. (2002). Extrusion process parameters, sensory characteristics, and structural properties of a high moisture soy protein meat analog. *Journal of Food Science, 67*(3), 1066–1072. https://doi.org/10.1111/j.1365-2621.2002.tb09454.x

Liu, K., & Hsieh, F.-H. (2008). Protein–protein interactions during high-moisture extrusion for fibrous meat analogues and comparison of protein solubility methods using different solvent systems. *Journal of Agricultural and Food Chemistry, 56*(8), 2681–2687. https://doi.org/10.1021/jf073343q

Liu, Y., Wang, D., Wang, J., Yang, Y., Zhang, L., Li, J., & Wang, S. (2020). Functional properties and structural characteristics of phosphorylated pea protein isolate. *International Journal of Food Science and Technology, 55*(5), 2002–2010. https://doi.org/10.1111/ijfs.14391

Martínez-Velasco, A., Lobato-Calleros, C., Hernández-Rodríguez, B. E., Román-Guerrero, A., Alvarez-Ramirez, J., & Vernon-Carter, E. J. (2018). High intensity ultrasound treatment of faba bean (*Vicia faba* L.) protein: Effect on surface properties, foaming ability and structural changes. *Ultrasonics Sonochemistry, 44*, 97–105. https://doi.org/10.1016/j.ultsonch.2018.02.007

McCarthy, N. A., Kennedy, D., Hogan, S. A., Kelly, P. M., Thapa, K., Murphy, K. M., & Fenelon, M. A. (2016). Emulsification properties of pea protein isolate using homogenization, microfluidization and ultrasonication. *Food Research International, 89*, 415–421. https://doi.org/10.1016/j.foodres.2016.07.024

McClements, D. J., & Grossmann, L. (2021). A brief review of the science behind the design of healthy and sustainable plant-based foods. *Npj Science of Food, 5*(1), 17. https://doi.org/10.1038/s41538-021-00099-y

McClements, D. J., & Grossmann, L. (2022). *Next-generation plant-based foods: Design, production, and properties*. Springer International Publishing. https://doi.org/10.1007/978-3-030-96764-2

Meng, A., Chen, F., Zhao, D., Wei, Y., & Zhang, B. (2022). Identifying changes in soybean protein properties during high-moisture extrusion processing using dead-stop operation. *Food Chemistry, 395*, Article 133599. https://doi.org/10.1016/j.foodchem.2022.133599

Mosibo, O. K., Ferrentino, G., Alam, M. R., Morozova, K., & Scampicchio, M. (2022). Extrusion cooking of protein-based products: Potentials and challenges. *Critical Reviews in Food Science and Nutrition, 62*(9), 2526–2547. https://doi.org/10.1080/10408398.2020.1854674

Nieuwland, M., Geerdink, P., Brier, P., van den Eijnden, P., Henket, J. T. M. M., Langelaan, M. L. P., Stroeks, N., van Deventer, H. C., & Martin, A. H. (2014). Reprint of "Food-grade electrospinning of proteins.". *Innovative Food Science & Emerging Technologies, 24*, 138–144. https://doi.org/10.1016/j.ifset.2014.07.006

Omosebi, M. O., Osundahunsi, O. F., & Fagbemi, T. N. (2018). Effect of extrusion on protein quality, antinutritional factors, and digestibility of complementary diet from quality protein maize and soybean protein concentrate. *Journal of Food Biochemistry, 42*(4), Article e12508. https://doi.org/10.1111/jfbc.12508

Osen, R., Toelstede, S., Eisner, P., & Schweiggert-Weisz, U. (2015). Effect of high moisture extrusion cooking on protein–protein interactions of pea (*Pisum sativum* L.) protein isolates. *International Journal of Food Science and Technology, 50*(6), 1390–1396. https://doi.org/10.1111/ijfs.12783

Othmeni, I., Karoui, R., & Blecker, C. (2024). Impact of pH on the structure, interfacial and foaming properties of pea protein isolate: Investigation of the structure – function relationship. *International Journal of Biological Macromolecules, 278*, Article 134818. https://doi.org/10.1016/j.ijbiomac.2024.134818

Ozturk, O. K., & Hamaker, B. R. (2023). Texturization of plant protein-based meat alternatives: Processing, base proteins, and other constructional ingredients. *Future Foods, 8*, Article 100248. https://doi.org/10.1016/j.fufo.2023.100248

Pöri, P., Nisov, A., & Nordlund, E. (2022). Enzymatic modification of oat protein concentrate with trans- and protein-glutaminase for increased fibrous structure formation during high-moisture extrusion processing. *Lebensmittel-Wissenschaft und -Technologie, 156*, Article 113035. https://doi.org/10.1016/j.lwt.2021.113035

Samard, S., & Ryu, G.-H. (2019). Physicochemical and functional characteristics of plant protein-based meat analogs. *Journal of Food Processing and Preservation, 43*(10), Article e14123. https://doi.org/10.1111/jfpp.14123

Shanthakumar, P., Klepacka, J., Bains, A., Chawla, P., Dhull, S. B., & Najda, A. (2022). The current situation of pea protein and its application in the food industry. *Molecules, 27*(16). https://doi.org/10.3390/molecules27165354. Article 16.

Shen, Y., & Li, Y. (2021). Acylation modification and/or guar gum conjugation enhanced functional properties of pea protein isolate. *Food Hydrocolloids, 117*, Article 106686. https://doi.org/10.1016/j.foodhyd.2021.106686

Shen, Y., Tang, X., & Li, Y. (2021). Drying methods affect physicochemical and functional properties of quinoa protein isolate. *Food Chemistry, 339*, Article 127823. https://doi.org/10.1016/j.foodchem.2020.127823

Souza Filho, P. F., Andersson, D., Ferreira, J. A., & Taherzadeh, M. J. (2019). Mycoprotein: Environmental impact and health aspects. *World Journal of Microbiology and Biotechnology, 35*(10), 147. https://doi.org/10.1007/s11274-019-2723-9

Sui, X., Zhang, T., & Jiang, L. (2021). Soy protein: Molecular structure revisited and recent advances in processing technologies. *Annual Review of Food Science and Technology, 12*(1), 119–147. https://doi.org/10.1146/annurev-food-062220-104405

Tang, X., Shen, Y., Zhang, Y., Schilling, M. W., & Li, Y. (2021). Parallel comparison of functional and physicochemical properties of common pulse proteins. *Lebensmittel-Wissenschaft und -Technologie, 146*, Article 111594. https://doi.org/10.1016/j.lwt.2021.111594

Tinus, T., Damour, M., Van Riel, V., & Sopade, P. A. (2012). Particle size-starch–protein digestibility relationships in cowpea (Vigna unguiculata). *Journal of Food Engineering, 113*(2), 254–264. https://doi.org/10.1016/j.jfoodeng.2012.05.041

Webb, D., Dogan, H., Li, Y., & Alavi, S. (2023a). Physico-chemical properties and texturization of pea, wheat and soy proteins using extrusion and their application in plant-based meat. *Foods, 12*(8), 1586. https://doi.org/10.3390/foods12081586

Webb, D., Dogan, H., Li, Y., & Alavi, S. (2023b). Use of legume flours and fiber for tailoring structure and texture of pea protein-based extruded meat alternatives. *Journal of Food Science, 88*(1), 57–71. https://doi.org/10.1111/1750-3841.16397

Willett, W., Rockström, J., Loken, B., Springmann, M., Lang, T., Vermeulen, S., Garnett, T., Tilman, D., DeClerck, F., Wood, A., Jonell, M., Clark, M., Gordon, L. J., Fanzo, J., Hawkes, C., Zurayk, R., Rivera, J. A., Vries, W. D., Sibanda, L. M., … Murray, C. J. L. (2019). Food in the Anthropocene: The EAT–Lancet Commission on healthy diets from sustainable food systems. *The Lancet, 393*(10170), 447–492. https://doi.org/10.1016/S0140-6736(18)31788-4

Xiao, C. W. (2008). Health effects of soy protein and isoflavones in Humans123. *The Journal of Nutrition, 138*(6), 1244S–1249S. https://doi.org/10.1093/jn/138.6.1244S

Yang, J., Duan, Y., Zhang, H., Huang, F., Wan, C., Cheng, C., Wang, L., Peng, D., & Deng, Q. (2023). Ultrasound coupled with weak alkali cycling-induced exchange of free sulfhydryl-disulfide bond for remodeling interfacial flexibility of flaxseed protein isolates. *Food Hydrocolloids, 140*, Article 108597. https://doi.org/10.1016/j.foodhyd.2023.108597

Zhang, B., Kang, X., Cheng, Y., Cui, B., & Abd El-Aty, A. M. (2022). Impact of high moisture contents on the structure and functional properties of pea protein isolate during extrusion. *Food Hydrocolloids, 127*, Article 107508. https://doi.org/10.1016/j.foodhyd.2022.107508

Zhang, J., Liu, L., Liu, H., Yoon, A., Rizvi, S. S. H., & Wang, Q. (2019). Changes in conformation and quality of vegetable protein during texturization process by extrusion. *Critical Reviews in Food Science and Nutrition, 59*(20), 3267–3280. https://doi.org/10.1080/10408398.2018.1487383

Zhang, Y., & Ryu, G. (2023). Effects of pea protein content and extrusion types on physicochemical properties and texture characteristic of meat analogs. *JSFA Reports, 3*(1), 30–40. https://doi.org/10.1002/jsf2.97

Zhang, T., Yu, S., Pan, Y., Li, H., Liu, X., & Cao, J. (2023). Properties of texturized protein and performance of different protein sources in the extrusion process: A review. *Food Research International, 174*, Article 113588. https://doi.org/10.1016/j.foodres.2023.113588

Zhang, X., Zhao, Y., Zhang, T., Zhang, Y., Jiang, L., & Sui, X. (2022). High moisture extrusion of soy protein and wheat gluten blend: An underlying mechanism for the formation of fibrous structures. *Lebensmittel-Wissenschaft und -Technologie, 163*, Article 113561. https://doi.org/10.1016/j.lwt.2022.113561

Zhu, Y.-S., Shuai, S., & FitzGerald, R. (2018). Mung bean proteins and peptides: Nutritional, functional and bioactive properties. *Food & Nutrition Research*. https://doi.org/10.29219/fnr.v62.1290